COBEM 2021 26th International Congress of Mechanical Engineering
ABCM Associação Brasileira de Engenharia e Ciências Mecânicas
November 22-26, 2021, Virtual Congress, Brazil

COB-2021-1106
EXPERIMENTAL VALIDATION OF A BOND GRAPH MODEL OF A SHAPE MEMORY ALLOY WIRE ACTUATOR

Lucas da Silva Olinda
Euripedes Guilherme de Oliveira Nobrega
Computational Mechanics Department, Mechanical Engineering Faculty, State University of Campinas - UNICAMP, Campinas (SP), Brazil. – Rua Mendeleyev, 200 - Cidade Universitária "Zeferino Vaz", Campinas, SP, Brazil. CEP:13083-860
l228250@dac.unicamp.br ; egon@fem.unicamp.br

Abstract. *Shape memory alloys (SMA) are smart materials that, after undergoing apparently plastic deformation, have the ability to recover their geometry when subjected to a thermal stimulus. However, the mathematical modeling of the SMA is complex due to its non-linear behavior, which make it difficult to simulate SMA-based actuated devices designs. Thus, this paper aims to develop and test a mathematical model of an SMA wire using the Bond Graph technique, a preferred way to facilitate modeling of multi-domain systems. For this purpose, an SMA wire with a diameter of 0.3 mm and a length of 250 mm was adopted as an actuator to be analyzed. To identify its respective parameters an experimental workbench was built to perform thermomechanical tests, applying heat through a controlled electrical current. After a number of excitation cycles, the wire acquired a stable behavior, then a series of experiments were conducted to identify the parameters that are used in the bond graph model. The model results were compared to those acquired using the experimental test bench, showing a good similarity between the respective values, such as the maximum displacement and the duration of heating and cooling of the actuator during each operating cycle, thus validating the complete procedure. Finally, a hydraulic SMA driven diaphragm minipump was designed and modeled, and will be developed in the next steps of this work.*

Keywords: *Shape memory alloy (SMA), bond graph, modeling, dynamic system*

1. INTRODUCTION

The shape memory alloys (SMA) are metallic alloys belonging to the subgroup of smart materials that have the characteristic of reversing a plastic deformation after undergoing thermal stimulus. This occurs due to the reversible phase transformation of the material, modifying the crystals structures (phases), being called martensite (lower temperature phase, can be easily deformed) and austenite (higher temperature phase, difficult to be deformed) (Mihálcz, 2001). These phase transformations are responsible for the phenomenon of the shape memory effect (SME) and superelasticity (SE) or pseudoelasticity.

The development of actuators using SMA encompasses several areas of engineering such as robotics, aerospace, biomedical, MEMS (micro-electro-mechanical systems) and structures and composites. One of the main attractions of this actuator is its great strength generated from a small amount of material, in addition to having a silent performance, which makes it advantageous in relation to the other conventional actuators such as electric motors, pneumatics and hydraulics (Mohd Jani *et al.*, 2014). Among the various materials that exhibit this behavior, such as Fe–Mn–Si, Cu–Zn–Al and Cu–Al–Ni alloys, the NiTi (Nitinol) received greater prominence for the development of applications due to its high ductility and tensile strength, in addition to being a material with good biocompatibility (Farber *et al.*, 2020; Choudhary and Kaur, 2016).

Mathematical models that describe the complex behavior of the SMA are fundamental for the development of applications. Since 1980, models representing the SMA have been widely researched. In recent years, a significant number of models have been developed using different methods such as cosine hardening rule or even exponential function to represent the phase transformation of the SMA (Lagoudas, 2008). However, modeling equipment that uses the SMA as an actuator usually results in complex systems because they involve different domains. An alternative to circumvent the difficulties of this development is using the bond graph technique.This is a multi-domain modeling technique based on the decomposition into basic components (resistive, capacitive and inertial). However, unlike the equivalent electrical circuit, bond graph uses a system with generalized components, facilitating the connection between different domains present in the device to be modeled. Applications of this approach can be analyzed in work such as (Bakka and Karimi, 2013) in which a wind turbine was modeled using the bond graph.

Then, the aim of this paper is to develop a mathematical model of an SMA wire using the bond graph technique. For this, a workbench was construct for training and extracting the wire parameters, necessary for the development of

the model. The martensitic fraction of the SMA was performed with model of (Ikuta *et al.*, 1991) and was included as a capacitive field in the system's bond graph. Finally, a hydraulic SMA driven diaphragm minipump was designed and modeled to illustrate a possible application of the actuator.

2. METHODOLOGY

In the present work, an SMA wire known as Flexinol, made of nickel-titanium (NiTi), produced by Dynalloy, Inc, with a diameter of 0.3 mm and a length of 250 mm was adopted. This wire was used as a reference for the development of the mathematical model, so an experimental workbench was made to carry out the training of this material and necessary tests to identify fundamental parameters for the model. Before starting the tests, the SMA wire was subjected to a heat treatment at a temperature of 450° C for 30 min to eliminate any possible hardening from the manufacturing process.

2.1 Construct of workbech

The workbench concept uses gravity to tension the SMA wire, in which a load cell is attached to the upper end of the wire while a load compartment exerts force on the other end. For the activation of the SMA wire, the use of electric current, based on the Joule effect for heating, was defined as it is a simple and easy control method, while a laser sensor measures the displacement of the wire according to the movement of the load. All signals are measured using a dSPACE data acquisition system and transmitted to a microcomputer for post-processing and plotting the results (Figure 1).

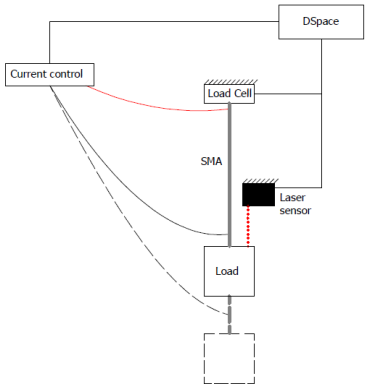

Figure 1. Iconic diagram of the workbench operation.

The external structure of the workbench, which may be seen in Fig. 2, was built in wood (MDF) to reduce the airflow influence on the wire, although it is not totally isolated of temperatures variations, in addition to provide general support for the experiment. The metallic object inside is simply used to adjust the direction of the displacement sensor, without exerting which does not interfere with the test.

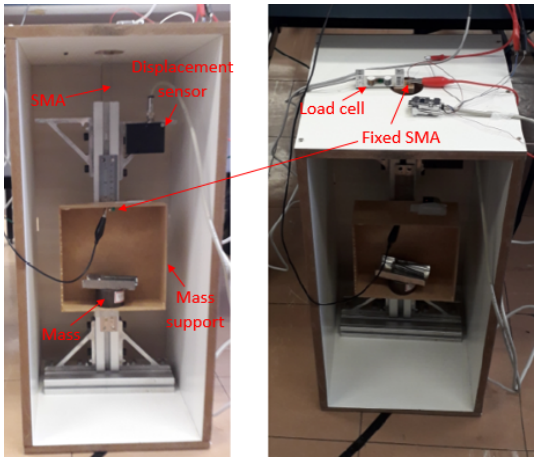

Figure 2. Experimental workbench built.

To control the system current, a circuit was created using a TIP122 transistor, a 20 W power resistor, and a DC source of 10 V. The source and SMA were connected in series to the transistor collector and the resistor was connected to the emitter. To control the current, the base of the transistor was powered by the acquisition board, in which the current

can be configured via software and adjusted as needed in the experiment. To identify the current through the SMA, the voltage across the power resistor was measured using the dSPACE, and performing the conversion through Ohm's law. For the load cell, an Teensy 3.1 microcontroller coupled to an amplifier converter HX711 for weight sensors was used, and its signal was converted and transmitted to the acquisition board through an analog signal. Both circuits were fixed to a universal breadboard PCB shown in Fig. 3.

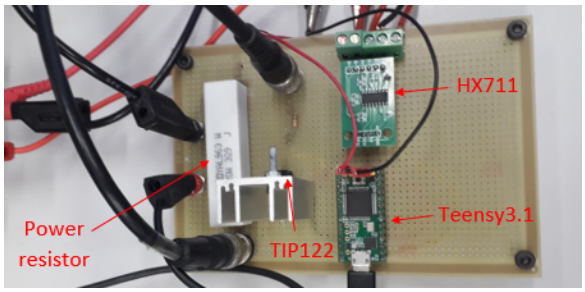

Figure 3. Electronic circuits fixed on a universal PCB.

Some heating and cooling cycles were performed on the SMA wire under mechanical tension, using a square wave signal of 0.7 A with a period of 100 s and a duty cycle of 25%, in order to ensure full displacement during the cycles. The axial load applied to the wire was changed as the cycles were carried out. Every 10 cycles, initially with 200 mg, a load of 200 mg was added until reaching a total of 1 Kg. Then, the reverse process was carried out, decreasing until the initial mass of 200 mg was returned. In this context, it was possible to identify the yarn stabilization trend and the maximum deformations for each weight used. Finally, a final test was carried out to analyze the displacement as a function of the current applied to the wire. Thus, cycles with triangle wave signals with a period of 100 s were applied, varying between 0 and 0.9 A, making it possible to identify the hysteresis of the material at each cycle performed.

2.2 Mathematical model of SMA

The development of the mathematical model of the SMA wire originates from obtaining the temperature of the material during the heating and cooling cycles. In order to avoid interference of a termometer sensor it was adopted the estimation of the temperature from the heat transfer equation associated with heating by electric current defined by (Leo, 2007):

$$\rho A c_p \frac{d\theta(t)}{dt} = i^2 R - hA_c[\theta(t) - \theta_\infty] \tag{1}$$

where θ, θ_∞, t, R, h, c_p, A, ρ, A_c and i are wire temperature, room temperature, time, electrical resistance per unit length, heat transfer coefficient, specific heat, area, specific mass, surface area by wire length and input current, respectively. Among the used parameters, the heat transfer coefficient (h) is more complex because it is influenced by several physical factors of the material. An approach similar to what is presented by (Talebi *et al.*, 2014), which describes the variation of the h of an SMA wire according to its temperature, is here adopted.

With the estimated wire temperature, it is possible to find the transformation temperatures based on the relationship between the displacements, measured during the tests, and the material temperature. Thus, the martensitic fraction could be calculated using the equations proposed by (Ikuta *et al.*, 1991), where Eq. (2) describes the heating process and Eq. (3) cooling:

$$\xi_m = \frac{\xi_{ma}}{1 + exp\left[\frac{6{,}2}{A_f - A_s}\left(T - \frac{A_s + A_f}{2}\right)\right]} \tag{2}$$

$$\xi_m = \frac{1 - \xi_{mr}}{1 + exp\left[\frac{6{,}2}{M_s - M_f}\left(T - \frac{M_s + M_f}{2}\right)\right]} + \xi_{mr} \tag{3}$$

where A_s and A_f represent the temperature of the starting and ending of the transformation from martensite into austenite and M_s and M_f represent the starting and ending temperatures from the austenite into martensite. ξ_{ma} indicates the fraction of martensite at the beginning of heating and ξ_{mr} the fraction of martensite at the beginning of cooling.

2.3 Workbench model

In the case under study, as shown in Fig. 4, a mass coupled at the loose end of the wire deforms the SMA due to the gravity force while the other end is fixed to the setup structure. Thus, when heated, the wire shortening lifts the load and, when cooled, it is deformed until it returns to its initial length.

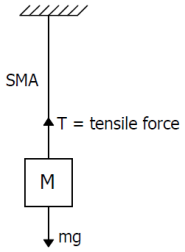

Figure 4. Iconic diagram of workbench.

To describe the mass and wire behavior, Fig. 5 presents three states to consider: the first state is the position of the mass in the complete austenite position (L), after moviment due to the current in the wire; the third state is the complete martensite position, after the current is interrupted, (L_{Max}); and the second state is represented by a point (X) between these two points when the current is applied and the mass is being lifted, with a deformation ΔL.

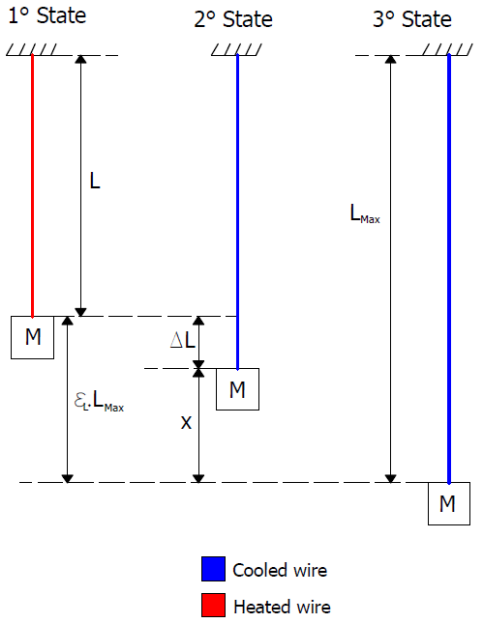

Figure 5. Diagram of SMA behavior in three states.

The term ϵ_L is the percentage of deformation between the first and third states, L_{Max} is the maximum length of the deformed wire and X represents the displacement generated by the wire movement. Thus, it is possible to estimate the force exerted by the SMA wire as in Eq. (4).

$$T = K\Delta L = K(\epsilon_L L_{Max} - x) \tag{4}$$

where K is the stiffness and can be found from the relationship between the stress and strain of the material. According to the works of (Romano and Tannuri, 2008; Xiaoguang *et al.*, 2017), the SMA mechanical behavior model can be defined as a function of the martensite fraction (ξ_m) as shown in Eq. (5):

$$\sigma = [(1 - \xi_m)E_a + \xi_m E_m]\epsilon \tag{5}$$

where E_a and E_m correspond to the modulus of elasticity in the austenite and martensite phase, respectively. Thus, replacing $\sigma = \frac{T}{A}$ and $\epsilon = \frac{\Delta L}{L}$:

$$T = [(1 - \xi_m)E_a + \xi_m E_m]\frac{A\Delta L}{L} \tag{6}$$

Comparing Eq.(6) with Eq. (4), the stiffness of the material can be defined as:

$$K = [(1 - \xi_m)E_a + \xi_m E_m]\frac{A}{L} \tag{7}$$

Thus, the dynamic model of the experimental workbench can be defined using the Newton's second law and adding a damping from the SMA wire itself.

$$M\ddot{x} + C\dot{x} + Kx = K\epsilon_L L_{Max} - mg \tag{8}$$

From the dynamic model, the system was modeled using the bond graph technique. The system model representation in bond graph can be observed in Fig. 6. Thus, following Eq. 8, each component of the system was represented by an element of the model. Mass was defined as an inertial element (I), damping as a resistive element (R) and the behavior of the SMA wire as a capacitive field (C) containing the Eq. 2, Eq. 3 and Eq. 4. Regarding the drive, the applied electric current was defined as a flow source modulated by a square wave (MSf) being linked to a gyrator element (GY) responsible for obtaining the wire temperature from Eq. 1. Furthermore, a source of effort (MSe) was implemented to represent the forces applied to the system as the force of gravity and of the SMA actuator. However, it can be observed that K is a parameter that defines both the elasticity and the force exerted by the SMA during its heating. So it was necessary to direct the value of K to the source of effort.

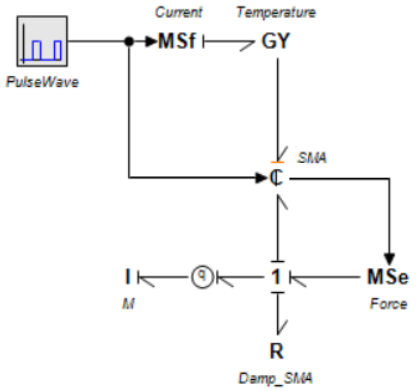

Figure 6. Bond graph from the experimental workbench.

2.4 Diaphragm minipump model

In order to develop an application using the SMA model, a hydraulic SMA driven diaphragm minipump was designed. The minipump structure and its respective driving the minipump are shown in Fig. 7. For activation, the SMA wire was fixed at the top and wound on pulleys to reduce the physical space of the device. The minipump was adjusted right below, so that one of the ends of the wire acts directly on the movement of the diaphragm, which is initially fully pressed. When heating, the SMA wire raises an elastic structure attached to the diaphragm, forcing the liquid suction into the chamber. The purpose of this structure is to exert a biasing force, which, after the heating current is interrupted, is sufficient to deform the SMA wire until the diaphragm returns to its full martensitic point, allowing an amount of fluid to move during the process.

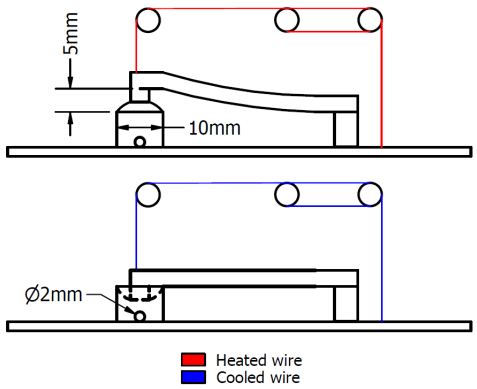

Figure 7. Iconic diagram of the hydraulic minipump with SMA wire actuation.

The liquid inlet and outlet channels were defined with lengths of 30 mm each, and an internal diameter of 2 mm. Both friction and fluid inertia were obtained through the Eq. (9) and Eq. (10), respectively. In addition, valves were used to

ensure flow direction, making it difficult for liquid to return in both the suction and pumping stages.

$$R = \frac{128\mu L}{\pi D_H^4} \tag{9}$$

$$I = \frac{\rho L}{A} \tag{10}$$

where, μ is the dynamic viscosity , L the channel length, D_H the hydraulic diameter, ρ the fluid density and A the channel cross-section.

The complete hydraulic minipump, represented in Fig. 8 is modeled using bond graph, where the SMA behavior is represented using the experimental model of the wire as identified in the workbench. The elastic structure is defined with a capacitive (C) and inertial (I) elements, the membrane is represented by a transformer (TF) and the input and output channels as resistive (R) and inertial (I) elements.

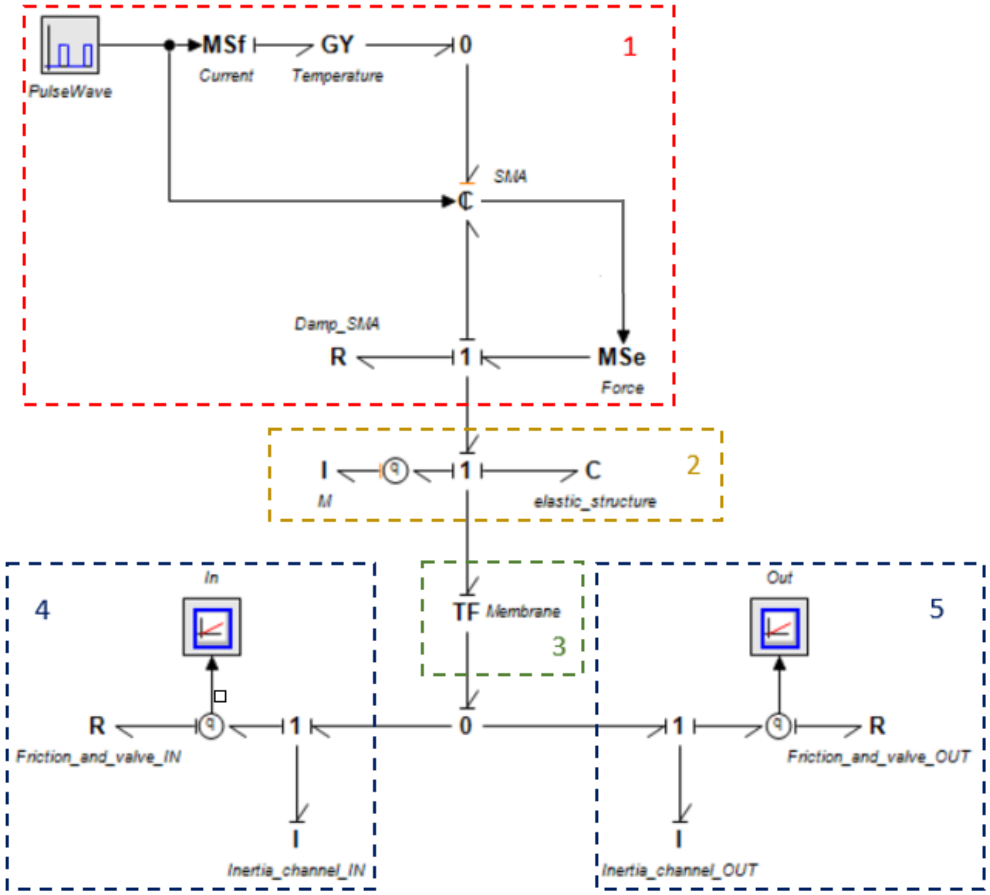

Figure 8. Bond graph of the hydraulic minipump: 1-SMA; 2-elastic structure; 3-membrane; 4-channel input; 5-channel output.

3. RESULTS

3.1 Experimental workbench

The SMA wire was stabilized through thermomechanical cycles with application of square wave signals, using the experimental workbench. After, triangular wave signals were applied to identify the hysteresis of the material. Figure 9 shows the behavior of the wire, after training, identifying the SMA hysteresis when plotting the displacement as a function of the system current variation. Graphs were separated according to the mass used in each test.

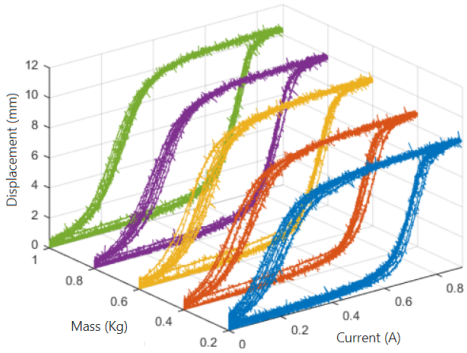

Figure 9. SMA deformation in relation to the applied current.

At the end of training, the wire acquired a stable behavior, reaching displacements of 8.5 mm (in the test with a mass of 0.2 kg) and 10.25 mm (in the test with a mass of 1 kg), generating deformations between 3.4 and 4.1% of the useful length of the wire. The model developed for the workbench used the tests with a load of 1 kg as a reference, because it provides a higher deformation of the SMA wire.

3.2 Parameters identification

The identification of the phase transformation temperatures of the SMA wire is of fundamental importance for the development of the mathematical model. The wire temperature was estimated using Eq. (1) with the values of the Tab. 1. Thus, as shown in Fig. 10, it is possible to find an approximation for each transformation temperature, analyzing the relationship between the length of the wire according to the temperature variation.

Table 1. Parameters used to calculate the SMA temperature.

Parameters	Symbols	Values
Room temperature	θ_∞	20 ° C
Wire diameter	d	0.3 mm
Wire length	L	250 mm
Specific heat	C_p	837 $\frac{J}{Kg.^\circ C}$
Resistance per unit length	R	11.32 Ω/m
Density	ρ	6450 $\frac{Kg}{m^3}$
Current	i	0.7 A

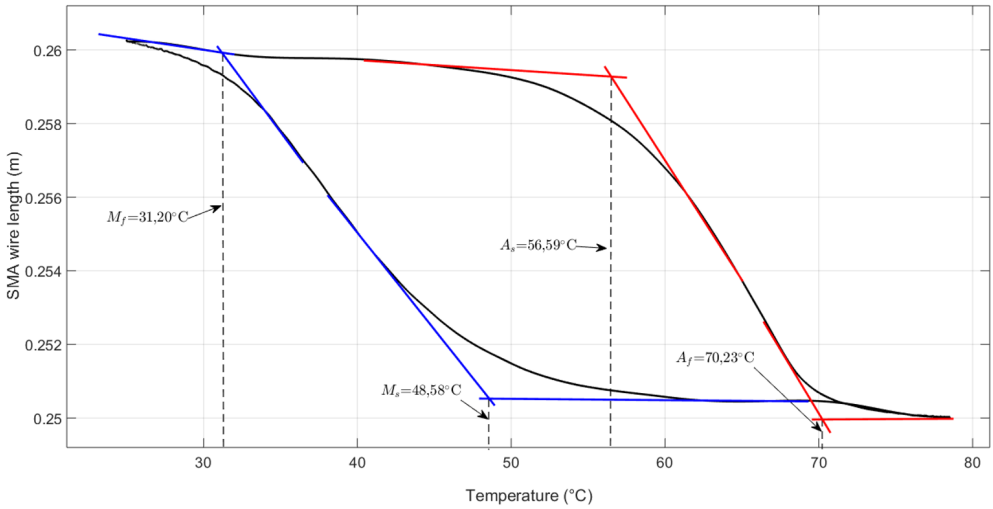

Figure 10. Transformation temperatures of SMA wires.

The transformation temperatures were estimated by drawing lines tangent to the curves contained in the thermomechanical cycle. The red lines get the temperatures during heating (initial and final austenite phase) while the blue ones

define them during cooling (initial and final martensite phase). Thus, the phase transformation temperatures were found: $A_s = 56.59°$ C, $A_f = 70.23°$ C, $M_s = 31.20°$ C and $M_f = 48.58°$ C.

With the defined parameters, the variation of the martensitic fraction of the wire was calculated using square wave signals of current of 0.7 A, in an analogous way to the training cycles. Figure 11 shows the variation of temperature and martensitic fraction of the SMA model using the identified transformation temperatures.

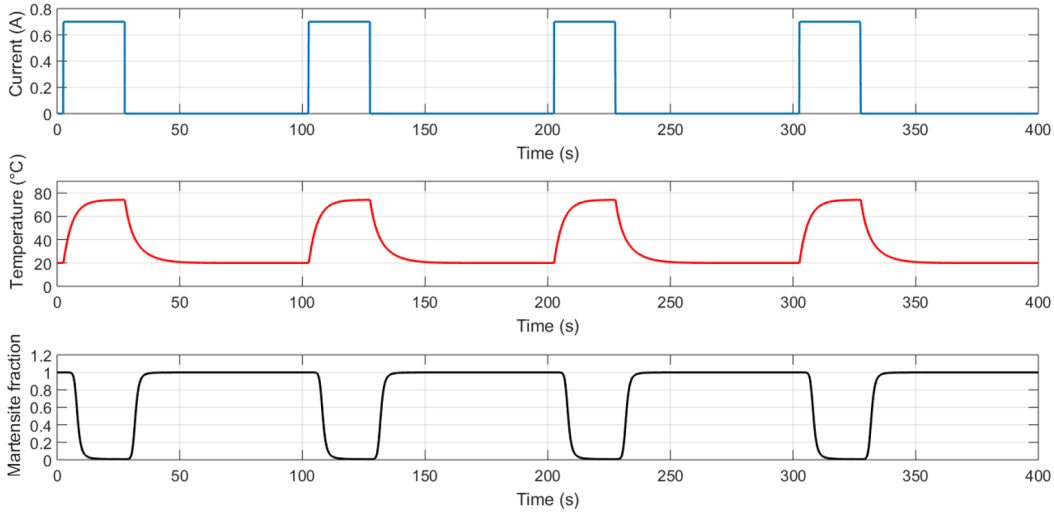

Figure 11. SMA wire drive model. Top: current, middle: temperature and bottom: martensite fraction.

For each applied current pulse, the wire acquired a temperature higher than A_f, completely transforming the martensite into austenite (martensite fraction with a value of 0). During cooling, the temperature reached a value lower than M_f, completely transforming the austenite into martensite (martensite fraction with a value of 1).

3.3 Model results using bond graph

The bond graph model of the system was created and simulated using the parameters in the Tab. 2. Fig. 12 shows the comparison between the simulated displacement and the experimentally measured result.

Table 2. Parameters used in the experimental workbench model.

Parameters	Values	Parameters	Values
A_f	70.23 °C	L_f	260.4 mm
A_s	56.59 °C	L	250 mm
M_f	31.20 °C	g	9.81 m/s^2
M_s	48.58 °C	c	100 $\frac{Ns}{m}$
E_m	3.2x10^9 Pa	M	1 Kg
E_a	86x10^9 Pa	d	0.3 mm

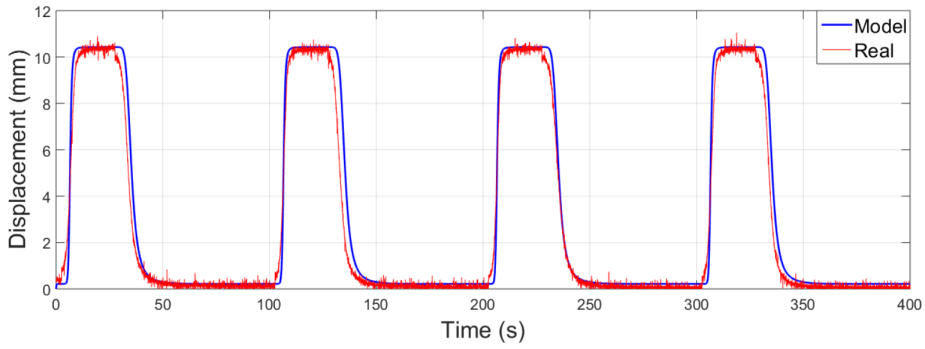

Figure 12. Comparison between the model displacement with the experimental result (real).

The result in Fig. 12 shows a small error for the displacement, denoting a good representation of the SMA wire behavior, as such, validating the model.

The hydraulic SMA drive diaphragm minipump was then modeled using the validated bond graph model. As the displacement required for the operation of the minipump is 5 mm, a length of 122 mm was defined to meet this characteristic. In addition, the SMA heating and cooling time was reduced, using 10 and 20 s, respectively, to higher system efficiency. The Fig. 13 shows the flow variation during the activation of the device, in addition to the amount of liquid transported by the minipump according to the parameters used in Tab. 3. The average flow rate of the system was estimated at 8.1 $\mu L/s$.

Table 3. Parameters used in model of the hydraulic SMA drive diaphragm minipump.

Parameters	**Values**
L	122 mm
L_f	127 mm
D_m	10 mm
$C_{structure}$	1962
$I_{structure}$	0.1
$R_{chanel/valve\_IN}$	$458.34x10^6$
$R_{chanel/valve\_OUT}$	$76.39x10^6$
$I_{IN/OUT}$	$15x10^3$

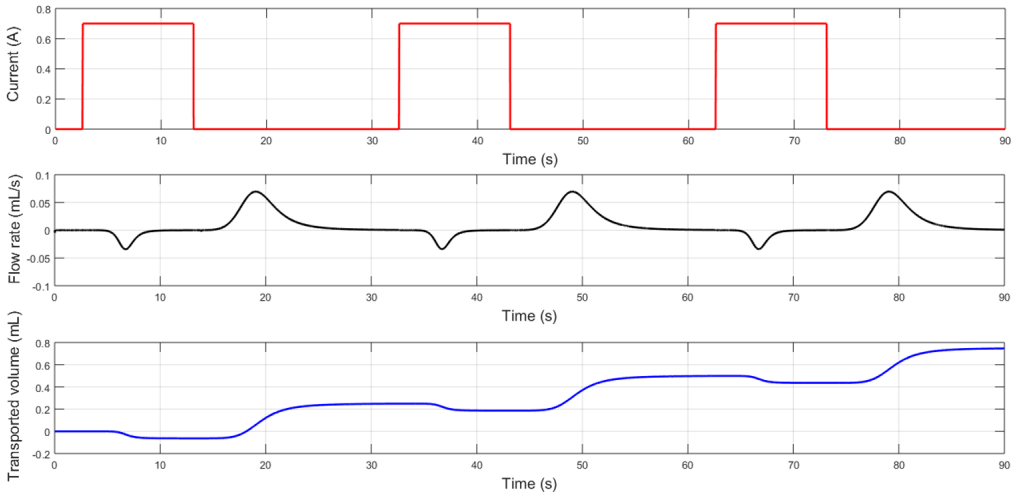

Figure 13. Minipump behavior during each actuation cycle.

4. CONCLUSION

As an important tool to represent multidomain systems, the bond graph technique is adopted in the present work to define a mathematically model for the behavior of an SMA wire as an actuator to project a minipump. The built workbench proved to be efficient for stabilizing the material, reaching displacements around 4% of the useful length of the SMA wire. The development of the bond graph model used the parameters identified through the bench, representing the behavior of the SMA wire. The displacement estimated by the proposed model was similar to that measured experimentally, enabling its validation. Finally, a hydraulic SMA diaphragm minipump with 1 cm of diameter was modeled, estimating a flow rate of 8.1 $\mu L/s$, using the proposed bond graph model of the wire actuator. Next steps in this research will be the construction and test of the designed minipump.

5. ACKNOWLEDGEMENTS

This study was financed in part by the Coordenação de Aperfeiçoamento de Pessoal de Nível Superior – Brasil (CAPES) – Finance Code 001.

6. REFERENCES

Bakka, T. and Karimi, H.R., 2013. "Bond graph modeling and simulation of wind turbine systems". Vol. 27, No. 6, pp. 1843–1852. ISSN 1976-3824. doi:10.1007/s12206-013-0435-x. URL https://doi.org/10.1007/s12206-013-0435-x.

Choudhary, N. and Kaur, D., 2016. "Shape memory alloy thin films and heterostructures for mems applications:

A review". Vol. 242, pp. 162–181. ISSN 0924-4247. doi:https://doi.org/10.1016/j.sna.2016.02.026. URL https://www.sciencedirect.com/science/article/pii/S0924424716300814.

Farber, E., Zhu, J.N., Popovich, A. and Popovich, V., 2020. "A review of niti shape memory alloy as a smart material produced by additive manufacturing". Vol. 30, pp. 761–767. ISSN 2214-7853. doi:https://doi.org/10.1016/j.matpr.2020.01.563. URL https://www.sciencedirect.com/science/article/pii/S2214785320306738. Materials Science: Composites, Alloys and Materials Chemistry.

Ikuta, K., Tsukamoto, M. and Hirose, S., 1991. "Mathematical model and experimental verification of shape memory alloy for designing micro actuator". In *[1991] Proceedings. IEEE Micro Electro Mechanical Systems*. pp. 103–108. doi:10.1109/MEMSYS.1991.114778.

Lagoudas, D., 2008. *Shape Memory Alloys: Modeling and Engineering Applications*. Springer US.

Leo, D.J., 2007. *Shape Memory Alloys*, John Wiley & Sons, Ltd, chapter 6, pp. 298–345. ISBN 9780470209721. doi:https://doi.org/10.1002/9780470209721.ch6. URL https://onlinelibrary.wiley.com/doi/abs/10.1002/9780470209721.ch6.

Mihálcz, I., 2001. "Fundamental characteristics and design method for nickel-titanium shape memory alloy". Vol. 45, pp. 75–86.

Mohd Jani, J., Leary, M., Subic, A. and Gibson, M.A., 2014. "A review of shape memory alloy research, applications and opportunities". Vol. 56, pp. 1078–1113. ISSN 0261-3069. doi:https://doi.org/10.1016/j.matdes.2013.11.084. URL https://www.sciencedirect.com/science/article/pii/S0261306913011345.

Romano, R. and Tannuri, E.A., 2008. "Modelagem e validação experimental de um atuador baseado em liga de memória de forma". Vol. 19, No. 1, pp. 30–42. ISSN 0103-1759. doi:https://doi.org/10.1590/S0103-17592008000100003.

Talebi, H., Golestanian, H., Zakerzadeh, M. and Homaei, H., 2014. "Thermoelectric heat transfer modeling of shape memory alloy actuators". In *The 22st Annual International Conference on Mechanical Engineering-ISME2014*.

Xiaoguang, L., Daohui, Z., Xingang, Z. and Han, J., 2017. "Modeling and control of shape memory alloy actuator using feedback linearization". In *2017 36th Chinese Control Conference (CCC)*. pp. 1222–1227. doi:10.23919/ChiCC.2017.8027516.

7. RESPONSIBILITY NOTICE

The author(s) is (are) solely responsible for the printed material included in this paper.